Progress In Electromagnetics Research, Vol. 123, 243–261, 2012

THE FAR FIELD TRANSFORMATION FOR THE ANTENNA MODELING BASED ON SPHERICAL ELECTRIC FIELD MEASUREMENTS

P. Li and L. Jiang*

Department of Electrical and Electronic Engineering, The University of Hong Kong, Pokfulam Road, Hong Kong, China

Abstract—According to the uniqueness theorem, the far field radiation pattern of radiators such as antennas can be determined from the measured tangential electric or magnetic field components over an arbitrary Huygens' surface enclosing the radiator. In this paper, a method using the spherical electric field measurement is developed to calculate the far field radiation. Following the Schelkunoff's field equivalence principle, a spherical region surrounding the radiator is assumed and its internal space is filled up with the perfect electric conductor (PEC). The radiated field from the Huygens' equivalent electric current is zero. Referring to the Ohm-Rayleigh method and the scattering wave superposition, the dyadic Green's function (DGF) with the presence of a PEC sphere is expanded by a series of spherical vector wave functions. Based on the DGF and the measured tangential electric field, the radiation behavior of the radiator can be directly predicted without involving the uncertainty from the inverse process. The robustness and accuracy of the proposed method are verified through several canonical antenna benchmarks.

1. INTRODUCTION

Followed by the near field data post processing, advanced near field measurement techniques are broadly employed today to characterize antenna related issues such as antenna diagnostics [1], far field (FF) predictions, and radiation pattern synthesis, etc.. For antennas with large aperture size or working at low frequencies, the direct far field measurement is expensive and difficult due to the space requirement for the anechoic chamber. Besides, the near field data contains very useful

Received 23 October 2011, Accepted 7 December 2011, Scheduled 22 December 2011
* Corresponding author: Lijun Jiang (ljiang@eee.hku.hk).

information for antenna diagnostics [2]. Traditional near-field far-field transformation (NF-FF) algorithms employ a set of equivalent sources that could be electric/magnetic dipoles, electric/magnetic current sources, or plane waves, etc..

In [3, 4], the equivalent magnetic current source over an infinite fictitious PEC plane in front of the antenna aperture is determined by the planar electric near field scanning, in which the resultant magnetic current is approximated by 2D pulse basis functions. A similar idea is proposed in [5], where the equivalent source is represented by a set of planar electric currents over a perfect magnetic conductor (PMC) plane. The effect of the PMC plane is considered through the image theory. The unknown equivalent sources are thereby solved by singular value decomposition. However, these ideas have a common deficiency: they only work for the half space radiation in front of the equivalent source plane. Plus, an inverse process is needed before the far field radiation calculation.

To overcome the aforementioned deficiency, researchers developed another method in which equivalent sources are distributed over a surface enclosing the radiator. In [6, 7], equivalent current sources are reconstructed over a spherical surface enclosing the antenna or on the surface of the antenna itself. The resultant equivalent current source can be used to characterize the full 3D radiation pattern. In [8], magnetic and electric dipoles are used as equivalent sources to approximate the original field. Both radiated fields from the reconstructed dipoles and measured near fields over a sphere are expanded into spherical harmonic functions. The expansion coefficients are solved by the mode matching method.

Although the above methods are eligible for the far field radiation, there is a significant discrepancy between the reconstructed current and the Love's equivalence current. This fact was first noticed by Persson and Gustafsson [9] and a more detailed treatment was proposed by Quijano and Vecchi [10–12] and Jorgensen et al. [13], etc. To obtain the correct Love's equivalent current, the field radiated by the equivalent source inside the Huygens' surface must be enforced to zero.

Another method for the NF-FF transformation is proposed to consider the full probe correction through the diagonal translation operator [15]. The equivalent currents are not calculated explicitly. Instead, they are expanded by plane waves. A further step in [16] is to discretize the equivalent currents by RWG basis functions and compute their coefficients through the fast multipole method.

In general, all above mentioned methods require the inverse scattering process, which solves equivalent sources before calculating the far field radiation. This usually suffers the loss of the evanescent

wave information and hence there is the uncertainty issue in the recovered equivalent sources.

In this paper, a technique based on the uniqueness theorem [14] is developed and verified. It avoids the conventional inverse scattering process but involves the explicit formulation of DGF. Only the tangential field measured on a spherical surface is employed to calculate the radiation directly through the analytical DGF of a PEC sphere [17]. Since the whole process is analytically rigorous except the field measurement, this method can precisely characterize the radiation from DUTs. It is necessary to clarify that our method is different from the modal expansion approach that expands the electric or magnetic field directly by a set of spherical wave functions while Green's function is never needed. However, adding the full probe correction into our approach is no trivial and further studies are needed. Hence, to avoid its influence, the probe shall be small enough and the measurement distance shall not be too close to the DUT to reduce the mutual coupling.

The organization of this paper is as follows: in Section 2, the proposed method is described with the analytical formula of DGF considering the presence of a PEC sphere. In Section 3, the proposed approach is applied to characterize the radiation of several representative antennas. Conclusions and discussions are presented at the end of the paper.

2. THEORY

One primary attraction of the conventional NF-FF transformation method is the employment of the free space DGF. But the uniqueness theorem indicates that only the tangential electric field or the tangential magnetic field on a closed boundary is needed to characterize the radiated field. It means that the measured tangential field on a closed surface can be used to calculate the radiation directly. But the corresponding DGF is difficult to find when it is not for the homogeneous free space. For many problems, the closed form DGF does not even exist. To avoid this issue and be general to most practical applications, we select a spherical surface as the measurement area to completely enclose the radiating sources.

As shown in Figure 1(a), the equivalence theorem [14] allows the field outside the measurement sphere calculated by the following expression [18]

$$\bar{E}(\bar{r})=\oiint_{s'}\left\{i\omega\mu\overline{\overline{G}}(\bar{r},\bar{r}')\cdot\left[\hat{n}\times\bar{H}(\bar{r}')\right]+\nabla\times\overline{\overline{G}}(\bar{r},\bar{r}')\cdot\left[\hat{n}\times\bar{E}(\bar{r}')\right]\right\}ds' \quad (1)$$

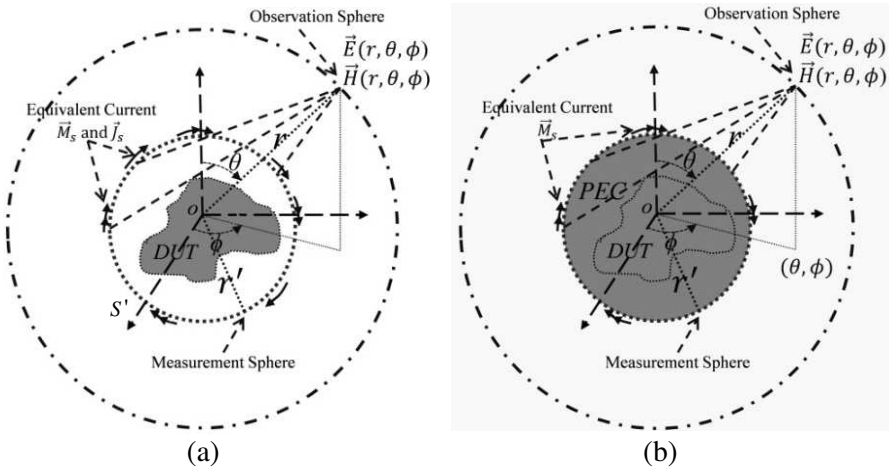

Figure 1. (a) Apply the equivalence theorem to the region outside the measurement spherical surface. (b) Following the Schelkunoff's equivalence principle, the region inside the measurement spherical surface is filled with PEC. Hence, only the magnetic current contributes to the radiated field outside the measurement sphere.

$$\bar{H}(\bar{r})=\iint_{s'}\left\{i\omega\varepsilon\overline{\overline{G}}(\bar{r},\bar{r}')\cdot\left[\bar{E}(\bar{r}')\times\hat{n}\right]+\nabla\times\overline{\overline{G}}(\bar{r},\bar{r}')\cdot\left[\hat{n}\times\bar{H}(\bar{r}')\right]\right\}ds' \quad (2)$$

where

$$\overline{\overline{G}}(\bar{r},\bar{r}')=\left(\overline{\overline{I}}+\frac{1}{k^2}\nabla\nabla\right)\frac{e^{ik|\bar{r}-\bar{r}'|}}{4\pi\,|\bar{r}-\bar{r}'|} \quad (3)$$

is the dyadic Green's function in the free space; $\hat{n}$ is the unit normal vector; $\hat{n}\times\bar{H}(\bar{r}')$ and $\bar{E}(\bar{r}')\times\hat{n}$ represent the equivalent tangential electric current and equivalent tangential magnetic current over the measurement sphere, respectively.

2.1. Dyadic Green's Function for a PEC Sphere

Since either electric field or magnetic field is needed to characterize the radiation based on the uniqueness theorem, only the tangential electric field is utilized in this paper. Following the Love's equivalence principle and Schelkunoff's equivalence principle [14], the field inside the measurement sphere is assumed to be zero. In this case, PEC is applied to fill the internal region of the measurement sphere, as shown in Figure 1(b). The contribution from the equivalent electric current in (1) becomes zero. Similarly, the second term on the right in (2) is equal to zero. However, the dyadic Green's function in (3) is altered

to consider the existence of the PEC sphere. The new formulae are written as

$$\bar{E}(\bar{r}) = \oiint_{s'} \left\{ \nabla \times \overline{\overline{G}}_{\mathrm{PEC}}(\bar{r}, \bar{r}') \cdot \left[\hat{n} \times \bar{E}(\bar{r}') \right] \right\} dS' \tag{4}$$

$$\bar{H}(\bar{r}) = \oiint_{s'} \left\{ i\omega\varepsilon \overline{\overline{G}}_{\mathrm{PEC}}(\bar{r}, \bar{r}') \cdot \left[\bar{E}(\bar{r}') \times \hat{n} \right] \right\} dS' \tag{5}$$

where, $\overline{\overline{G}}_{\mathrm{PEC}}(\bar{r}, \bar{r}')$ is the DGF with the presence of a PEC sphere enclosing the DUT at the origin. By the Ohm-Rayleigh method and the scattering wave superposition, $\overline{\overline{G}}_{\mathrm{PEC}}(\bar{r}, \bar{r}')$ can be formulated by two terms

$$\overline{\overline{G}}_{\mathrm{PEC}}(\bar{r}, \bar{r}') = \overline{\overline{G}}(\bar{r}, \bar{r}') + \overline{\overline{G}}_s(r, \bar{r}') \tag{6}$$

The first term $\overline{\overline{G}}(\bar{r}, \bar{r}')$ is the free space DGF and the second term $\overline{\overline{G}}_s(\bar{r}, \bar{r}')$ represents the scattering from the PEC sphere. Next, spherical vector wave functions are employed to expand the free space DGF. It is well known that the vector wave functions $\bar{L}_{mn}$, $\bar{M}_{mn}$ and $\bar{N}_{mn}$ make up a group of complete orthogonal basis. The divergence free electromagnetic fields can be expressed by the linear combination of $\bar{M}_{mn}$ and $\bar{N}_{mn}$ while $\bar{L}_{mn}$ represents the curl free field. In the spherical coordinate, $\bar{M}_{mn}$ and $\bar{N}_{mn}$ are solved as follows

$$\bar{M}_{mn} = \hat{e}_\theta \frac{im}{\sin\theta} B_n(kr) P_n^m(\cos\theta) e^{im\phi} - \hat{e}_\phi B_n(kr) \frac{\partial P_n^m(\cos\theta)}{\partial\theta} e^{im\phi} \tag{7}$$

$$\begin{aligned} \bar{N}_{mn} = {} & \hat{e}_r \frac{n(n+1)}{kr} B_n(kr) P_n^m(\cos\theta) e^{im\phi} \\ & + \frac{1}{kr} \frac{\partial(krB_n(kr))}{\partial(kr)} e^{im\phi} \left[\hat{e}_\theta \frac{\partial P_n^m(\cos\theta)}{\partial\theta} + \hat{e}_\phi \frac{im}{\sin\theta} P_n^m(\cos\theta) \right] \end{aligned} \tag{8}$$

The vector wave functions are then used to represent the $\overline{\overline{G}}(\bar{r}, \bar{r}')$ and $\overline{\overline{G}}_s(\bar{r}, \bar{r}')$ in (6) as follows [17, 19]

$$\begin{aligned} \overline{\overline{G}}(\bar{r}, \bar{r}') = {} & -\frac{1}{k} \hat{r}\hat{r} \delta(\bar{r} - \bar{r}') + \frac{ik}{4\pi} \sum_{n=1}^{\infty} \sum_{m=-n}^{n} C_{nm} \\ & \cdot \begin{cases} \left[\bar{M}_{mn}^{(1)}(k, \bar{r}) \bar{M}'_{mn}(k, \bar{r}') + \bar{N}_{mn}^{(1)}(k, \bar{r}) \bar{N}'_{mn}(k, \bar{r}') \right], \\ \qquad\qquad\qquad\qquad r > r' \\ \left[\bar{M}_{mn}(k, \bar{r}) \bar{M}'^{(1)}_{mn}(k, \bar{r}') + \bar{N}_{mn}(k, \bar{r}) \bar{N}'^{(1)}_{mn}(k, \bar{r}') \right], \\ \qquad\qquad\qquad\qquad r < r' \end{cases} \end{aligned} \tag{9}$$

$$\overline{\overline{G}}_s(\bar{r},\bar{r}') = \frac{ik}{4\pi}\sum_{n=1}^{\infty}\sum_{m=-n}^{n} C_{nm}\left[a_n \bar{M}_{mn}^{(1)}(k,\bar{r})\bar{M}'^{(1)}_{mn}(k,\bar{r}')\right.$$

$$\left.+b_n \bar{N}_{mn}^{(1)}(k,\bar{r})\bar{N}'^{(1)}_{mn}(k,\bar{r}')\right] \tag{10}$$

where $\bar{r}$ and $\bar{r}'$ are defined as the observation and current source position vectors. The coefficient C_{mn} is

$$C_{mn} = \frac{2n+1}{n(n+1)} \times \frac{(n-m)!}{(n+m)!} \tag{11}$$

The coefficients a_n and b_n in (10) are determined by applying the dyadic Dirichlet boundary condition on the PEC spherical surface which is

$$\hat{r} \times \overline{\overline{G}}_{\mathrm{PEC}}(\bar{r},\bar{r}')\,|_{r=r'} = 0 \tag{12}$$

It yields

$$a_n = -\frac{j_n(\rho)}{h_n^{(2)}(\rho)} \tag{13a}$$

$$b_n = -\frac{\frac{\partial}{\partial\rho}\left[\rho j_n(\rho)\right]}{\frac{\partial}{\partial\rho}\left[\rho h_n^{(2)}(\rho)\right]}, \quad \rho = kr' \tag{13b}$$

where r' is the radius of the PEC sphere. $j_n(\rho)$ and $h_n^{(2)}(\rho)$ are the first kind spherical Bessel function and second kind spherical Hankel function, respectively. The superscript $^{(1)}$ in (9) and (10) denotes that in (7) and (8) $B_n(kr) = h_n^{(2)}(kr)$, which represents outgoing waves; otherwise, $B_n(kr) = j_n(kr)$ for standing waves when $r \to 0$. In the far field region, approximations can be made as follows [20]

$$h_n^{(2)}(kr) \approx j^{n+1}\frac{e^{-jkr}}{kr} \tag{14a}$$

$$\frac{1}{kr}\frac{\partial\left[h_n^{(2)}(kr)kr\right]}{\partial(kr)} \approx j^n \frac{e^{-jkr}}{kr} \tag{14b}$$

However, when the observation point and/or the source point are located at the north or south poles ($\theta = 0,\ \pi$), the proposed method will suffer singularity problems due to the two terms in (15) contained in spherical wave functions. The detailed treatment is presented in the Appendix.

$$Q_1 = \frac{P_n^m(\cos\theta)}{\sin\theta}, \quad \text{and} \quad Q_2 = \frac{\partial P_n^m(\cos\theta)}{\partial\theta} \tag{15}$$

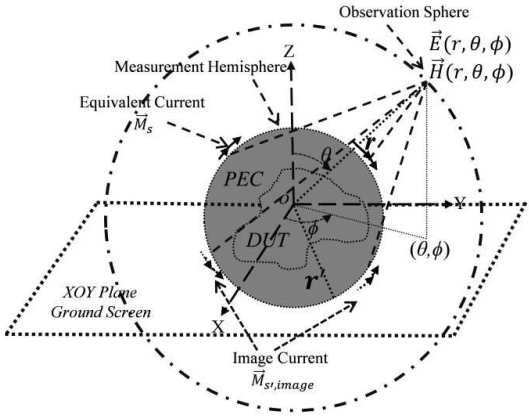

Figure 2. DUT placed on an infinite PEC ground. The electric field measurement is conducted over the upper hemisphere. The ground plane is removed by applying the image theorem.

2.2. Dyadic Green's Function for a PEC Hemisphere on an Infinite PEC Ground

Sometimes DUTs are placed on the PEC ground. For instance, the EMC/EMI evaluations of vehicles and aircrafts are often conducted in semi-anechoic chambers or at the open area test sites (OATS). Then only the hemispherical electric field scanning is needed. The influence of the PEC ground is counted by applying the image theory, as shown in Figure 2. The DGF in (6) is used for the field radiated by the current on the upper hemisphere. As for the radiation of the image source, the coordinate (r', θ', ϕ') is redefined as (r'', θ'', ϕ'') to represent the image current source position

$$\begin{cases} r'' = r' \\ \theta'' = \pi - \theta' \\ \phi'' = \phi' \end{cases} \tag{16}$$

2.3. Characterization of the Radiated Field by the Tangential Electric Field

The aforementioned DGF is applied to characterize electromagnetic emissions from antennas, PCBs and electronic devices, etc.. The compact form of DGF is as follows

$$\overline{\overline{G}}_{\mathrm{PEC}} = \begin{cases} \overline{\overline{G}}(\bar{r}, \bar{r}') + \overline{\overline{G}}_s(\bar{r}, \bar{r}'), & \text{for original source} \\ \overline{\overline{G}}(\bar{r}, \bar{r''}) + \overline{\overline{G}}_s(\bar{r}, \bar{r''}), & \text{for image source} \end{cases} \tag{17}$$

The tangential electric field is acquired on a fictitious PEC sphere with regular measurement intervals $\Delta\theta$ and $\Delta\phi$. The impressed tangential magnetic current can be calculated by

$$\bar{M}_{\theta' i,j} = -\hat{r'}_{i,j} \times \bar{E}_{\phi'}(a, \theta'_i, \phi'_j) \tag{18}$$

$$\bar{M}_{\phi' i,j} = -\hat{r'}_{i,j} \times \bar{E}_{\theta'}(a, \theta'_i, \phi'_j) \tag{19}$$

where $(a,\ \theta'_i,\ \phi'_j)$ is the spherical coordinate of the measurement position. a is the radius of the sphere,and the angles are defined as

$$\theta'_i = \left(i - \frac{1}{2}\right)\Delta\theta, \quad i = 1, 2, \ldots, N_\theta \tag{20a}$$

$$\phi'_j = \left(j - \frac{1}{2}\right)\Delta\phi, \quad j = 1, 2, \ldots, N_\phi \tag{20b}$$

where N_θ and N_ϕ are numbers of sampling points. Then, the magnetic current components $\bar{M}_\theta$ and $\bar{M}_\phi$ are represented by the pulse basis functions

$$\bar{M}_\theta = \sum_{i=1}^{N_\theta}\sum_{j=1}^{N_\phi} \bar{J}_{\theta' i,j}\Pi_{i,j}(a, \theta', \phi') \tag{21a}$$

$$\bar{M}_\phi = \sum_{i=1}^{N_\theta}\sum_{j=1}^{N_\phi} \bar{J}_{\phi' i,j}\Pi_{i,j}(a, \theta', \phi') \tag{21b}$$

where $\Pi_{i,j}(a, \theta', \phi')$ is the pulse function defined as

$$\Pi_{i,j}(a, \theta', \phi') = \begin{cases} 1, & \text{if } \begin{cases} \theta_i - \frac{\Delta\theta}{2} \le \theta' \le \theta_i + \frac{\Delta\theta}{2} \\ \phi_i - \frac{\Delta\phi}{2} \le \phi' \le \phi_i + \frac{\Delta\phi}{2} \end{cases} \\ 0 & \text{otherwise} \end{cases} \tag{22}$$

For DUTs placed on an infinite ground, the image magnetic currents are directly given by

$$\bar{M}_{\theta''} = -\sum_{i=1}^{N_\theta}\sum_{j=1}^{N_\phi} \bar{J}_{\theta' i,j}\Pi_{i,j}(a, \pi - \theta', \phi') \tag{23a}$$

$$\bar{M}_{\phi''} = \sum_{i=1}^{N_\theta}\sum_{j=1}^{N_\phi} \bar{J}_{\phi' i,j}\Pi_{i,j}(a, \pi - \theta', \phi') \tag{23b}$$

3. NUMERICAL RESULTS

Several benchmarks are used to investigate the applicability of the proposed methodology for the antenna radiation characterization.

3.1. The Pyramid Horn Antenna in the Free Space

A horn antenna [21] in Figure 3 operating at 1.645 GHz is studied. Its aperture size is 55 by 42.8 cm^2. For methodology validation purposes, the measured tangential electric field data over a spherical surface with radius equal to 2 m is obtained by the numerical calculation of an commercial full-wave simulation software FEKO [21]. 2592 field points are acquired with 5 degrees angular resolution in both theta and phi directions. Comparing the far field data $\bar{E}_{ref,n}$ directly simulated from FEKO with the calculated far field $\bar{E}_{trans,n}$ based on the proposed method, we have the following far field error definition

$$\sigma_{\text{MSE}} = 10\log_{10}\frac{\sum_{n=1}^{N}\left\|\left|\bar{E}_{trans,n}\right| - \left|\bar{E}_{ref,n}\right|\right\|^2}{\sum_{n=1}^{N}\left\|\bar{E}_{ref,n}\right\|^2} \tag{24}$$

where N is the number of measurements. $\|\,\|$ represents the induced norm and

$$\left|\bar{E}\right| = \sqrt{|E_\theta|^2 + |E_\phi|^2} \tag{25}$$

represents the magnitude of tangential electric components.

Figure 4 shows the computational time and the calculation error versus the truncation order. It can be observed that the minimum error happens around $N = 20$ while there is a slight increase for larger

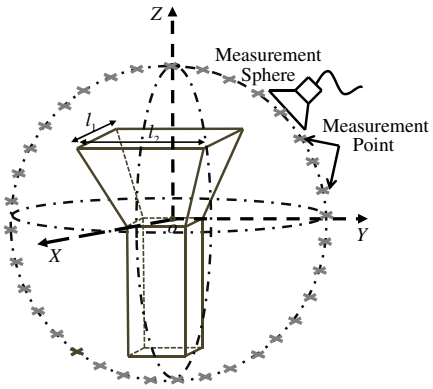

Figure 3. The geometry of the horn antenna and its measurement scenario.

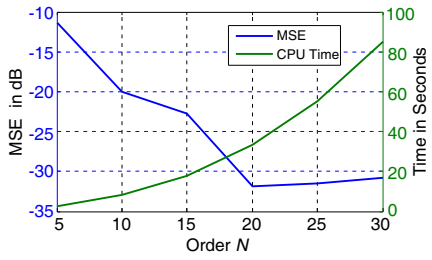

Figure 4. The error function MSE and the CPU time versus the order of the spherical wave functions.

N. The increasing error can be explained by the modal expansion and the finite discretization of the integral equation in (4). The equivalent magnetic current $\hat{r}' \times \bar{E}(\bar{r}')$ implicitly contains eigen modes that can also be expanded by spherical vector wave functions:

$$\hat{r}' \times \bar{E}(\bar{r}') = \hat{r}' \times \sum_{n'=1}^{\infty} \sum_{m'=-n}^{n} \left(Q_{1m'n'} \bar{M}^{(1)}_{m'n'}(\bar{r}') + Q_{2m'n'} \bar{N}^{(1)}_{m'n'}(\bar{r}') \right) \quad (26)$$

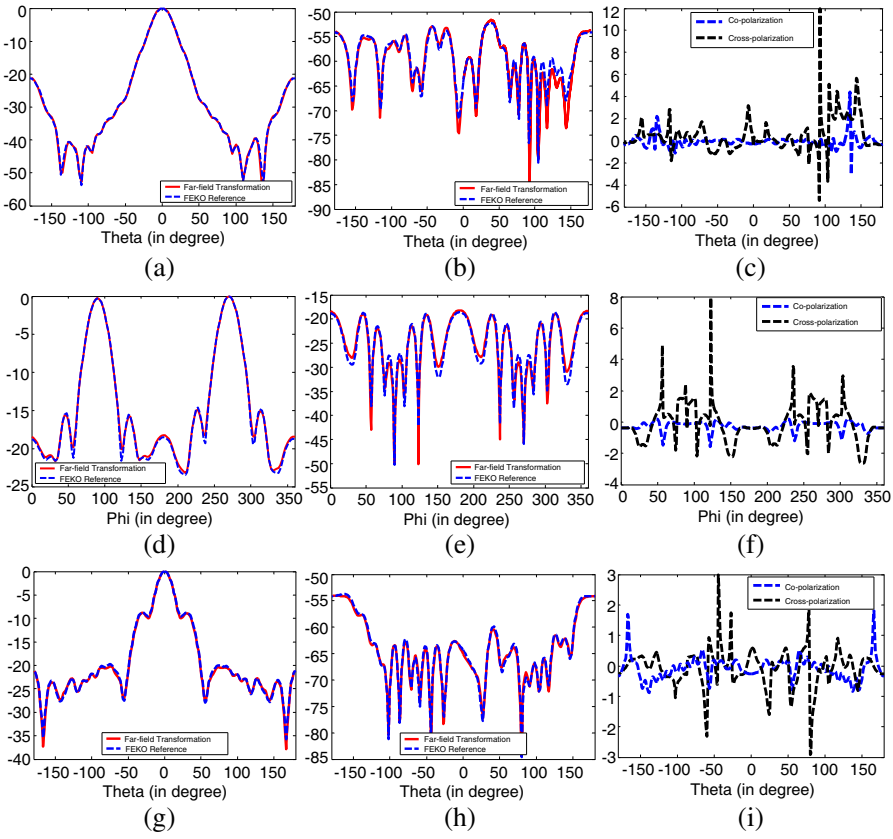

Figure 5. The normalized far field pattern with truncation order $N = 20$. (a) Co-polarization in XOZ plane. (b) Cross polarization in XOZ plane. (c) The difference (in dB) between the predicted result and the reference. (d) Co-polarization in XOY plane. (e) Cross polarization in XOY plane. (f) The difference (in dB) between the predicted result and the reference. (g) Co-polarization in YOZ plane. (h) Cross polarization in YOZ plane. (i) The difference (in dB) between the predicted result and the reference.

By substituting (26), (10) and (9) in (4), due to orthogonal properties of spherical vector wave functions, magnetic current contributions from each mode is computed and summed to form the total scattered field. For any radiator, its energy is focused on limited number of eigen modes. Because of the finite discretization and limited sampling, the modes with very weak magnitude will be overwhelmed by the noise introduced by the discretization. Hence, if a proper representation of the equivalent magnetic current can be approximated by N_J modes,

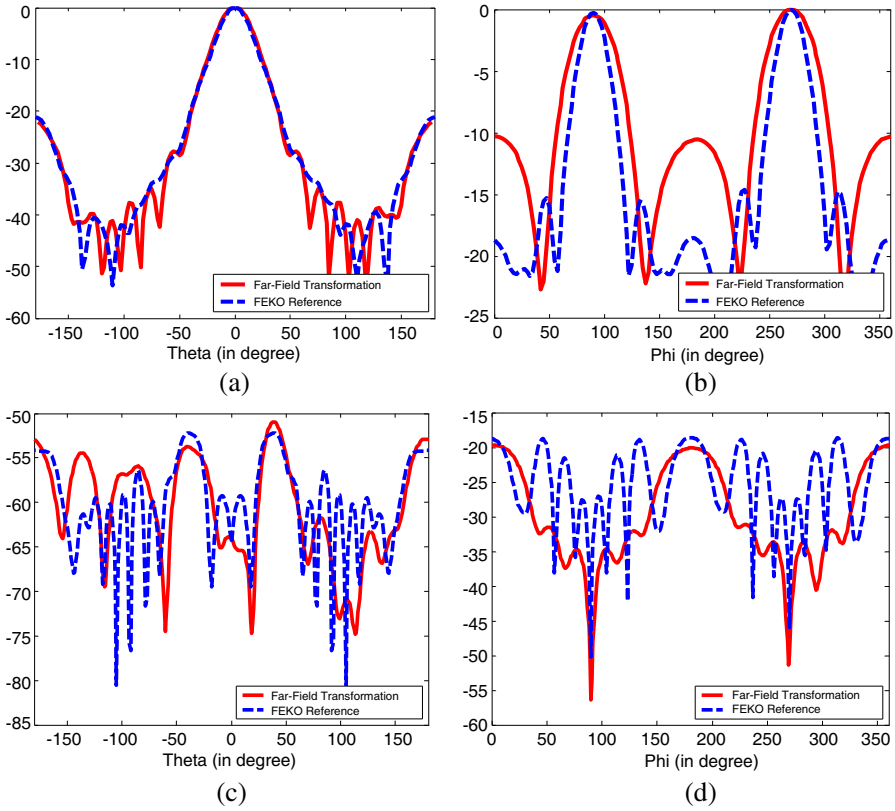

Figure 6. The normalized far field pattern with truncation order $N = 10$. (a) Co-polarization in XOZ plane. (b) Cross polarization in XOZ plane. (c) Co-polarization in XOY plane. (d) Cross polarization in XOY plane.

Equation (26) becomes

$$\hat{r}' \times \bar{E}(\bar{r}') = \hat{r}' \times \left[\sum_{n'=1}^{N_J} \sum_{m'=-n}^{n} \left(Q_{1m'n'} \bar{M}^{(1)}_{m'n'}(\bar{r}') + Q_{2m'n'} \bar{N}^{(1)}_{m'n'}(\bar{r}') \right) + \bar{E}_{error}(\bar{r}') \right] \quad (27)$$

where $\hat{r}' \times \bar{E}_{\text{error}}(\bar{r}')$ is the term containing weak eigen modes and discretization error. Then suppose the truncation number of the dyadic Green's function is set to N. When $N < N_J$, the overall error will decrease with increasing N. But when $N > N_J$, the error introduced by the discretization will introduce new residual errors that cannot be canceled by the orthogonal property. And this error will increase further with bigger N. But this increasing rate will become gradually slower because the magnitude of the higher order spherical vector wave functions decreases. The above statement is proved by employing Hertzian dipole that is a special case with $N_J = 1$. It can be seen that increasing N will cause error increase after $N = 1$. Raising the sampling rate will decrease the error significantly.

The far field radiation patterns from the proposed method are compared with the direct simulation by FEKO and shown in Figure 5. The differences between them are also presented. They agree with each other very well in both the vertical and horizontal planes. The cross polarization patterns also get very good agreements even though they are very weak.

To have an quantitative understanding of the effects of the spherical wave function truncation order, Figure 6 presents the results with the truncation order $N = 10$. Significant discrepancies can be observed. It reminds us that the truncation order of spherical wave

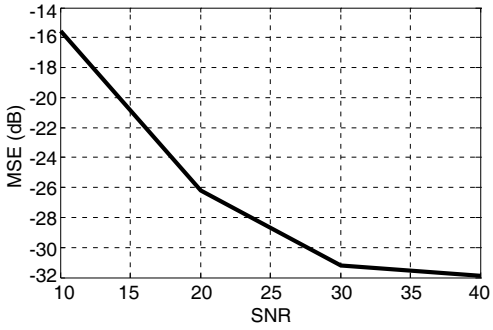

Figure 7. Mean squared errors for various SNRs using the far field transformation technique proposed in this paper.

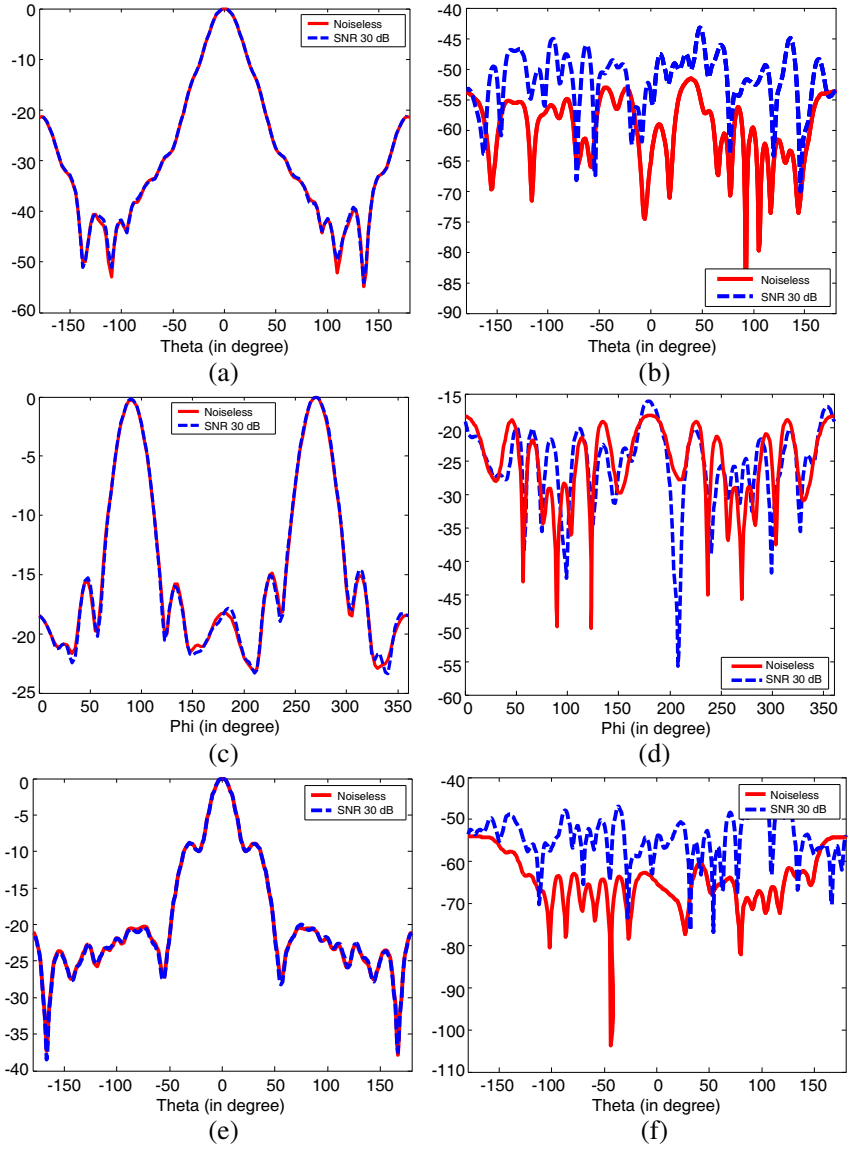

Figure 8. Normalized far field pattern utilizing field data with SNR = 30 dB. (a) Co-polarization in XOZ plane. (b) Cross polarization in XOZ plane. (c) Co-polarization in XOY plane. (d) Cross polarization in XOY plane. (e) Co-polarization in YOZ plane. (f) Cross polarization in YOZ plane.

functions must be picked up properly. For most practical purposes, a proper truncation number for acceptable error is given by the empirical rule [22]

$$N = [kr_0] + n_0 \tag{28}$$

where k is the wave number, r_0 is radius of the minimum sphere enclosing the antenna, the square bracket indicates the largest integer smaller than or equal to kr_0, the integer n_0 depends on the accuracy required. For example, in our benchmark, we took $N = 20$ with $n_0 = 5$ that is very close to the prediction in (28).

The imperfections in the real measurement environment, such as cable influences, positioning errors, reflections from absorbing walls, and probe errors could affect the accuracy of the radiated field evaluation. Hence, noise contaminated electric field data is employed to study this issue. Uncorrelated complex white Gaussian noise regularized by the signal-to-noise ratio (SNR) is stochastically added to the simulated noise free data. To have a better understanding of the influence, the MSE in dB defined in (24) is employed as an indicator again.

In Figure 7, the MSEs obtained by embedding different noise levels into the simulated data are presented. It shows that the influence of noises with SNR higher than 20 dB is negligible, while errors become more significant when the SNR of the measured field reaches 10 dB or below.

Figure 8 shows the transformed far field radiation pattern using the noise polluted data. The results explicitly indicate that the noise 30 dB lower than the original field data has negligible influence on the co-polarized far field pattern, whereas the cross polarization is distorted. The reason for this can be attributed to the weak cross-polarization which is more sensitive to numerical errors.

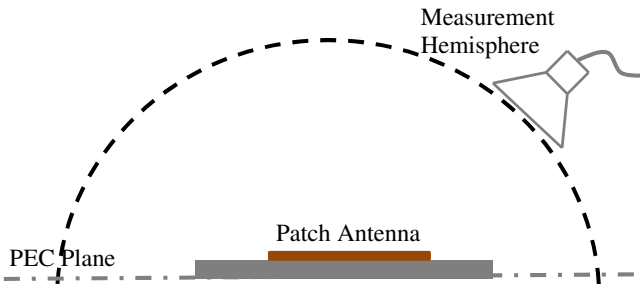

Figure 9. Measurement setup for a patch antenna over a PEC ground.

3.2. Effects of the Infinite Ground Plane

To investigate the case with the infinite PEC ground plane, a coaxially-fed microstrip patch antenna (Figure 9) [21] working at 2.85 GHz is studied. The simulated tangential electric field is obtained over a hemisphere with radius equal to 1 m. 1296 points are measured over the upper-hemisphere. The influence of the PEC ground is considered by the image theory in the proposed approach.

Normalized far field patterns over the upper hemisphere are calculated from the proposed approach and compared with the FEKO's direct simulation. The results are presented in Figure 10. Excellent agreements have been achieved. To clearly illustrate the PEC ground plane effect on the radiation pattern, the radiated electric field at 10 meters away from the origin without normalization is given in Figure 11. It shows that the ground plane has larger impact when the observation point is closer to the horizontal plane, as shown in Figure 11(c). The maximum error is about 6 dB.

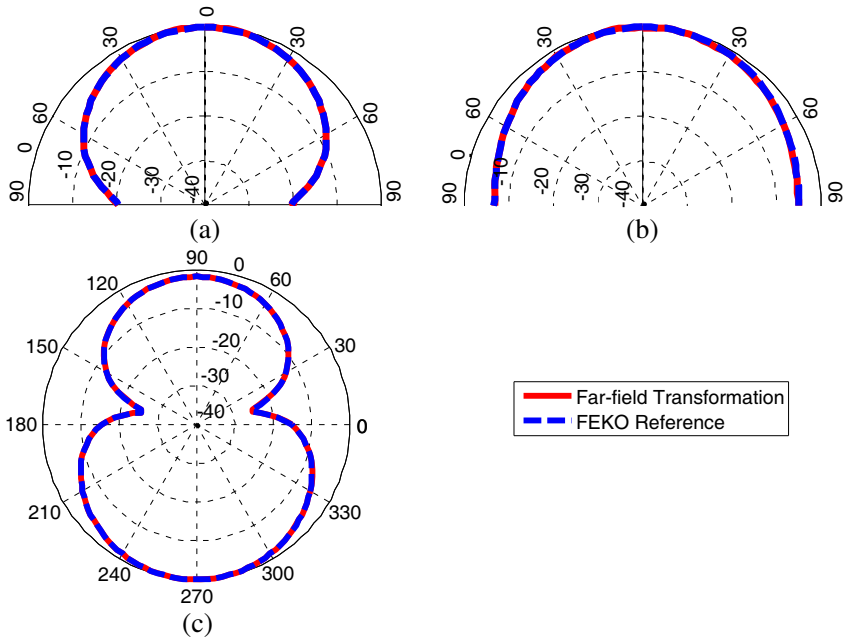

Figure 10. Transformed far-field pattern as well as FEKO reference. (a) Vertical cut in XOZ plane. (b) Vertical cut in YOZ plane. (c) Horizontal cut in XOY plane.

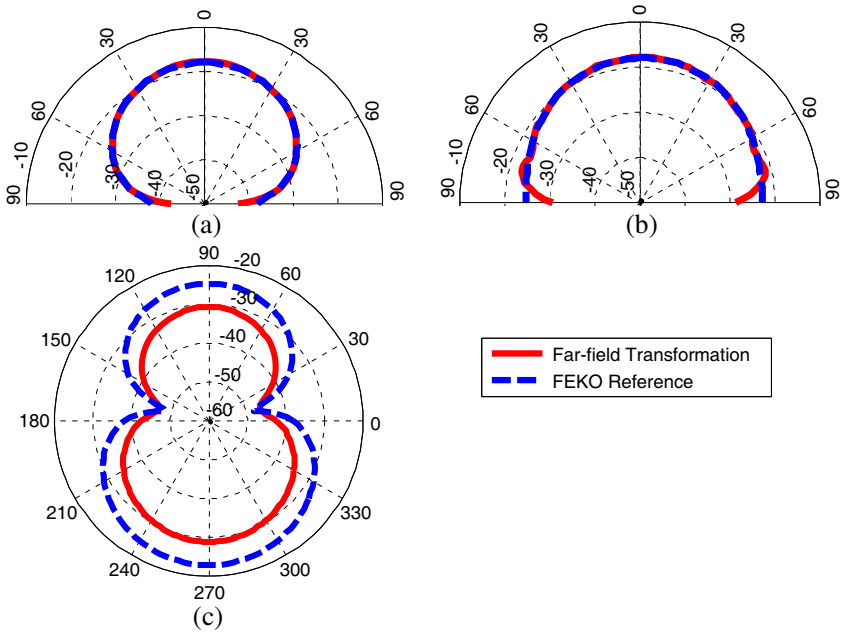

Figure 11. Amplitude of electric-field (dB) at $r = 10$ meters. (a) Vertical cut in XOZ plane. (b) Vertical cut in YOZ plane. (c) Horizontal cut in XOY plane.

4. CONCLUSION

A novel method based on the spherical electric field measurements is presented to model the radiated field from antennas and electronic devices. The explicit dyadic Green's function considering the presence of a PEC sphere is employed to avoid the conventional inverse scattering process. The accuracy of the proposed method is benchmarked for antenna problems. The robustness of the algorithm against possible measurement errors is carefully investigated and discussed. This method avoids the null space accuracy distortion of conventional inverse scattering based methods and works for general complex radiators.

ACKNOWLEDGMENT

We thank Professor W. C. Chew for his constructive suggestions. Also we are grateful to the supports from HKU Seed Fund 201001159006, and HKU Small Project Fund 201007176196, and the University Grant Council (AoE/P-04/08).

APPENDIX A.

To solve the singularity issue in (15) when $\theta = 0$ or π, let $x = \cos\theta$. Then

$$P_n^m(x) = \frac{1}{2^n n!}(1-x^2)^{m/2}\frac{\partial^{n+m}}{\partial x^{n+m}}(x^2-1)^n \tag{A1}$$

When $m \geq 2$,

$$\frac{P_n^m(x)}{\sin\theta} = \frac{1}{2^n n!}(\sin\theta)^{m-1}\frac{\partial^{n+m}}{\partial x^{n+m}}(x^2-1)^n = 0 \tag{A2}$$

For $m = 0$, the associated Legendre polynomial becomes the general Legendre polynomial. The singularity seems very difficult to be removed. However we notice that only the product of m with the singular term in (15a) is needed for Equations (11)–(14). Hence, for $m = 0$

$$m \cdot \frac{P_n^m(x)}{\sin\theta} = 0 \tag{A3}$$

for $m = 1$,

$$\begin{aligned}\frac{P_n^m(x)}{\sin\theta} &= \frac{1}{2^n n!}\frac{\partial^{n+m}}{\partial x^{n+m}}(x^2-1)^n \\ &= \frac{1}{2^n}\sum_{k=0}^{\lfloor n/2\rfloor}(-1)^k\frac{(2n-2k)!(n-2k)}{k!(n-k)!(n-2k)!}x^{n-2k-1}\end{aligned} \tag{A4}$$

As to the singular term in (15b), by referring the property of the general Legendre polynomial, the circumstance $m = 0$ is described as

$$\frac{\partial P_n(x)}{\partial\theta} = -\sin\theta\frac{\partial P_n(x)}{\partial x} = 0 \tag{A5}$$

Then, for $m \geq 1$,

$$\begin{aligned}\frac{\partial P_n^m(x)}{\partial\theta} &= -\sin\theta\frac{\partial P_n^m(x)}{\partial x} = -(n+1)\frac{P_n^m(x)}{\sin\theta}x \\ &\quad +(n-m+1)\frac{P_{n+1}^m(x)}{\sin\theta}\end{aligned} \tag{A6}$$

Based on the results shown in (A2), the result in (A6) equal to zero when $m \geq 2$. For $m = 1$, we can refer to the formula in (A4)

$$\begin{aligned}&\frac{\partial P_n^m(\cos\theta)}{\partial\theta} \\ &= -(n+1)\cos\theta\frac{1}{2^n}\times\sum_{k=0}^{\lfloor n/2\rfloor}(-1)^k\frac{(2n-2k)!(n-2k)!}{k!(n-k)!(n-2k)!}(\cos\theta)^{n-2k-1} \\ &\quad +\frac{n}{2^{n+1}}\times\sum_{k=0}^{\lfloor n/2\rfloor}(-1)^k\frac{[2(n+1)-2k]!}{k!(n+1-k)!(n-2k)!}(\cos\theta)^{n-2k}\end{aligned} \tag{A7}$$

REFERENCES

1. Laurin, J. J., J. F. Zurcher, and F. Gardiol, "Near-field diagnostics of small printed antennas using the equivalent magnetic current approach," *IEEE Trans. Antennas Propag.*, Vol. 49, No. 5, 814–828, May 2001.
2. Weng, H., D. Beetner, R. E. Dubroff, and J. Shi, "Estimation of high frequency currents from the near-field scan measurement," *IEEE Trans. Electromagn. Compat.*, Vol. 49, No. 4, Nov. 2007.
3. Peter, P. and T. K. Sarkar, "Planar near-field to far-field transformation using an equivalent magnetic current approach," *IEEE Trans. Antennas Propag.*, Vol. 40, No. 11, 1348–1356, Nov. 1992.
4. Taaghol, A. and T. K. Sarkar, "Near-field to near/far-field transformation for arbitrary near-field geometry utilizing an equivalent magnetic current," *IEEE Trans. Antennas Propag.*, Vol. 38, No. 3, 536–542, Aug. 1996.
5. Sarkar, T. K. and A. Taaghol, "Near-field to near/far-field transformation for arbitrary near-field geometry utilizing an equivalent electric current and MOM," *IEEE Trans. Antennas Propag.*, Vol. 47, No. 3, 566–573, Mar. 1999.
6. Alvarez, Y., F. Las-Heras, and M. R. Pino, "Reconstruction of equivalent currents distribution over arbitrary three-dimensional surfaces based on integral equation algorithms," *IEEE Trans. Antennas Propag.*, Vol. 55, No. 12, 3460–3468, Nov. 2007.
7. Alvarez, Y., F. Las-Heras, M. R. Pino, and T. K. Sarkar, "An improved super-resolution source reconstruction method," *IEEE Trans. Antennas Propag.*, Vol. 58, No. 11, 3855–3866, Nov. 2009.
8. Serhir, M., P. Besnier, and M. Drissim, "An accurate equivalent behavioral model of antenna radiation using a mode-matching technique based on spherical near field measurements," *IEEE Trans. Antennas Propag.*, Vol. 56, No. 1, 48–57, Jan. 2008.
9. Persson, K. and M. Gustafsson, "Reconstruction of equivalent currents using a near-field data transformation with radome applications," *Progress In Electromagnetics Research*, Vol. 54, 179–198, 2005.
10. Quijano, J. L. A. and G. Vecchi, "Improved-accuracy source reconstruction on arbitrary 3-D surfaces," *IEEE Antennas and Wireless Propagation Letters*, Vol. 8, 1046–1049, Sep. 2009.
11. Quijano, J. L. A. and G. Vecchi, "Field and source equivalence in source reconstruction on 3D surfaces," *Progress In Electromagnetics Research*, Vol. 103, 67–100, 2010.

12. Quijano, J. L. A. and G. Vecchi, "Near- and very near-field accuracy in 3-D source reconstruction," *IEEE Antennas and Wireless Propagation Letters*, Vol. 9, 634–637, Jul. 2010.
13. Jorgensen, E., P. Meincke, and M. Sabbadini, "Improved source reconstruction technique for antenna diagnostics," *Proc. 32nd ESA Antenna Workshop*, The Netherlands, Oct. 2010.
14. Rengarajan, S. R. and Y. Rahmat-Samii, "The field equivalence principle: Illustration of the establishment of the non-intuitive null fields," *IEEE Antennas and Propagation Magazine*, Vol. 42, No. 4, 122–128, Aug. 2000.
15. Schmidt, C. H., M. M. Leibfritz, and T. F. Eibert, "Fully probe-corrected near-field far-field transformation employing plane wave expansion and diagonal translation operators," *IEEE Trans. Antennas Propag.*, Vol. 56, No. 3, 737–746, Mar. 2008.
16. Eibert, T. F. and C. H. Schmidt, "Multilevel fast multipole accelerated inverse equivalent current method employing Rao-Wilton-Glisson discretization of electric and magnetic surface currents," *IEEE Trans. Antennas Propag.*, Vol. 57, No. 4, 737–746, Apr. 2009.
17. Tai, C.-T., *Dyadic Green Functions in Electromagnetic Theory*, 2nd Edition, IEEE Press, 1994.
18. Kong, J. A., *Electromagnetic Wave Theory*, EMW Publishing, Cambridge, Massachusetts, USA, 2008.
19. Chew, W. C., *Waves and Fields in Inhomogeneous Media*, Wiley, IEEE Press, 1999, ISBN 9780470547052.
20. Koivisto, P., "Reduction of errors in antenna radiation patterns using optimally truncated spherical wave expansion," *Progress In Electromagnetics Research*, Vol. 47, 313–333, 2004.
21. EM Software and Systems, FEKO Suite 5.2. Available: http://www.feko.info.
22. Hansen, J. E., *Spherical Near-Field Antenna Measurements*, Peter Peregrinus, London, 1998.